

Detection and sizing of cracks using potential drop techniques based on electromagnetic induction

Yasumoto SATO^{1*} and Hoon KIM²

¹ *Research Instruments Development Division, Toyota Central R&D Labs., Inc., 41-1, Yokomichi, Nagakute, Aichi 480-1192, Japan*

² *School of Mechanical and Automotive Engineering, Chonnam National University, San 96-1 Dundeock, Yeosu, Chonnam, 550-747, Korea*

ABSTRACT

The potential drop techniques based on electromagnetic induction are classified into induced current focused potential drop (ICFPD) technique and remotely induced current potential drop (RICPD) technique. The possibility of numerical simulation of the techniques is investigated and the applicability of these techniques to the measurement of defects in conductive materials is presented. Finite element analysis (FEA) for the RICPD measurements on the plate specimen containing back wall slits is performed and calculated results by FEA show good agreement with experimental results. Detection limit of the RICPD technique in depth of back wall slits can also be estimated by FEA. Detection and sizing of artificial defects in parent and welded materials are successfully performed by the ICFPD technique. Applicability of these techniques to detection of cracks in field components is investigated, and most of the cracks in the components investigated are successfully detected by the ICFPD and RICPD techniques.

KEYWORDS

nondestructive inspection, crack, potential drop technique, induced current, finite element analysis

ARTICLE INFORMATION

Article history:

Received 8 January 2011

Accepted 9 May 2011

1. Introduction

Large machines and structures such as nuclear power plants, airplanes, and chemical plants are required to have high reliability to ensure safety and soundness. The materials used may have some flaws occurring from manufacturing processes, and components have defects due to machining and weld processes. Also, components are operated under severe environments such as load, vibration, high pressure, high temperature, chemicals, and radiation for a long time. An ageing degradation is occurred in components due to the complex operation environments. The ageing degradation reduces the life-span of structures and can result in accidents that cause economic loss, environmental pollution, and personal injury [1].

In some of the large structures, damage tolerance design have been adopted in which operation are permitted with the existence of defects under the condition that safety margins are ensured while carrying out a safety evaluation. Therefore, to ensure the safety margins of structures, it is important that defects are detected and evaluated before the safety is affected [2].

Evaluation factors for defects include position, size, and shape. It is difficult to detect and evaluate these factors prior to failure under continuous field operating conditions. In order to detect existing defects in structures, nondestructive inspection techniques using radiation, ultrasound, magnetic field, electric current, and laser have been developed. Many researchers have continuously endeavored to improve the inspection sensitivity and accuracy of these techniques, and detect defects with non-contact methods [3, 4, 5].

Nondestructive inspection techniques that use an electric current to detect defects within conductive materials had been developed and called as potential drop (PD) techniques. These techniques are divided in two categories; direct current potential drop (DCPD) and alternating current potential drop (ACPD) [6, 7]. Generally, measurements are performed using a pair of current injection terminals and a pair of PD pick-up terminals. The terminals use spring loaded pins to scan a detection area. However, incomplete contact of current injection terminals can negatively affect the data. To avoid this negative effect of current injection of conventional PD technique, PD techniques based on electromagnetic induction have been developed that utilizes a current induced in the local

* Corresponding author, E-mail: yasumoto-sato@mosk.tytlabs.co.jp

detection area without contact it using a current exciter, and the applicability of the techniques has been investigated for some kinds of defects [8, 9, 10, 11]. However, the importance of numerical simulation of the technique and the applicability of the technique to detection of defects in real field components have not been investigated.

In this study, the PD techniques based on electromagnetic induction are applied to measurements of artificial defects in parent and weld metals, and cracks in real field components. An important role of numerical simulation in the data evaluation and interpretation of the PD technique based on electromagnetic induction are also described.

2. Potential drop technique based on electromagnetic induction

2.1. Principle of the PD technique based on electromagnetic induction

When an electric wire or a coil in which an alternating current flows is located near conductive materials, an electrical current is induced due to electromagnetic induction. The PD technique based on electromagnetic induction measures the PD due to the perturbation of this induced current which occurs as a result of defects.

The PD technique based on electromagnetic induction can be classified into induced current focused potential drop (ICFPD) technique and remotely induced current potential drop (RICPD) technique according to the exciter used in each of the probes.

The ICFPD technique utilizes a conductive wire as an exciter (induction wire) which is located near the surface of conductive material inspected. Correspondingly, the measurements are performed using relatively small currents, but the influence of the surface irregularity of the material measured is large.

The RICPD technique uses a coil as an exciter which is positioned 30 mm away from the surface of conductive material inspected. It is expected that the influence of the surface irregularity of the material on the measured PD is relatively small and the scattering superposed on the measured PD can be reduced.

Fig. 1 shows schematic illustrations of typical sensors for the PD technique based on electromagnetic induction.

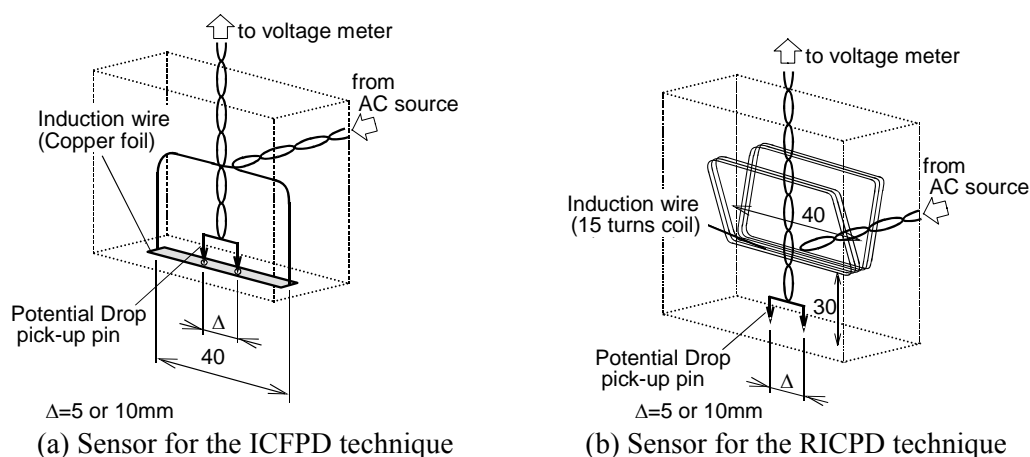


Fig. 1. Schematic illustrations of typical sensors for the PD techniques based on electromagnetic induction

2.2. Potential drop distributions around cracks

Schematics of PD distributions, which will be obtained by the PD techniques based on electromagnetic induction around defects, are shown in Fig. 2, along with the illustrations of induced current density distribution and the location of the PD pick-up pins of the sensor. The figures are drawn according to the interpretations of PD distributions for surface cracks [8] and for back wall cracks [10]. The shape of the PD distribution is independent of the exciter location of the sensor from

the surface of a conductive material under measurement because a way of an induced current flow is also independent of the exciter location.

For surface cracks, the PD distribution shows a complicated shape around the crack. Measured PD decreases as the sensor moves toward the crack until one of the PD pick-up pins of the sensor located just beside the crack because of the low current density region at the crack edge (position ① in Fig. 2(a)). The PD jumps up when one of the PD pick-up pins crosses the crack since the length of the induced current path increased (position ② in Fig. 2(a)). The PD distribution measured while the PD pick-up pins are across the crack shows U-shape due to changes in the effect of the low current density region between the PD pick-up pins on the measured PD.

For back wall or internal cracks, the PD distribution shows a convex shape and the maximum PD is measured when the sensor is located just above the crack (position ③ in Fig. 2(b)). This is because there is a high current density region at the tip of the crack.

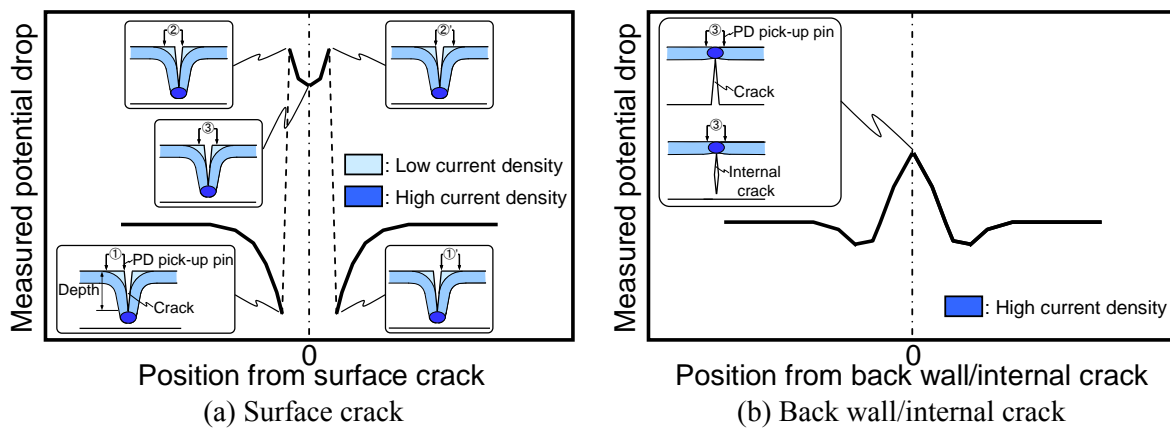


Fig. 2. Schematic illustrations of potential drop distributions measured around different cracks

3. Numerical simulation of the PD technique based on electromagnetic induction

For the PD technique based on electromagnetic induction, induced current distribution may change due to several experimental parameters such as shape of measured materials, depth and length of cracks, shape and size of exciter used in the sensor and skin depth of induced current, since the current is induced to the material under measurement. It is very difficult to evaluate these effects on the measured PDs by experiments, and numerical simulation is essential to evaluate these effects on the measured PDs. In this section, numerical simulation of the PD technique based on electromagnetic induction using finite element analysis (FEA) is presented.

The software used was a commercially available electromagnetic FEA cord (ANSYS Emag). The software allows users to analyze physical phenomenon of electromagnetic induction in solid under ac field based on $A-\phi$ (magnetic vector potential - electric scalar potential) method using edge elements. Governing equations for the $A-\phi$ method are;

$$\nabla \times \frac{1}{\mu} \nabla \times \mathbf{A} + \sigma \left(\frac{\partial \mathbf{A}}{\partial t} + \nabla \phi \right) = \mathbf{J}_s \quad (1)$$

$$\nabla \cdot \left(\mathbf{J}_s - \sigma \left(\frac{\partial \mathbf{A}}{\partial t} + \nabla \phi \right) \right) = 0 \quad (2)$$

where μ , σ and \mathbf{J}_s are permeability of material under the investigation, conductivity and source current density.

The exciter used in the RICPD sensor is located 30 mm away from the surface of conductive material under measurement, and therefore, extremely small meshes are not required for the finite element model of the RICPD technique comparing with the ICFPD technique whose exciter is

positioned near the surface of the conductive material under measurement. Accordingly, following investigation focuses on the analysis of the RICPD technique.

3.1. Simulation conditions

A schematic of a model analyzed by FEA is shown in Fig. 3. The model consists of a plate specimen of type 304 stainless steel (SS) containing 2D back wall slits with several depths (d), an induction coil and air surrounding the specimen and the coil. As the model is symmetrical, one-half of the model was used for the FEA. Two-dimensional back wall slits were modeled using elements with same electromagnetic properties of air. The specimen was divided into 9 elements in the thickness direction, 55 elements in longitudinal direction and 14 elements in width direction. Total number of elements and nodes including those of air were 46,322 and 198,777, respectively. Finite element mesh of the specimen and the coil is presented in Fig. 4. The electromagnetic properties used for the FEA are listed in Table 1.

Current density of $5 \times 10^6 \text{ A/m}^2$ was applied to the meshes of induction coil as an exciting current. Sizes of the air region surrounding the specimen and the coil are three times larger than those of the specimen and the coil that is enough to model the far field decay of magnetic field. On the symmetry plane (X-Y plane) to which the magnetic flux is normal, no constraints of degree of freedom were required, because it is the natural boundary condition.

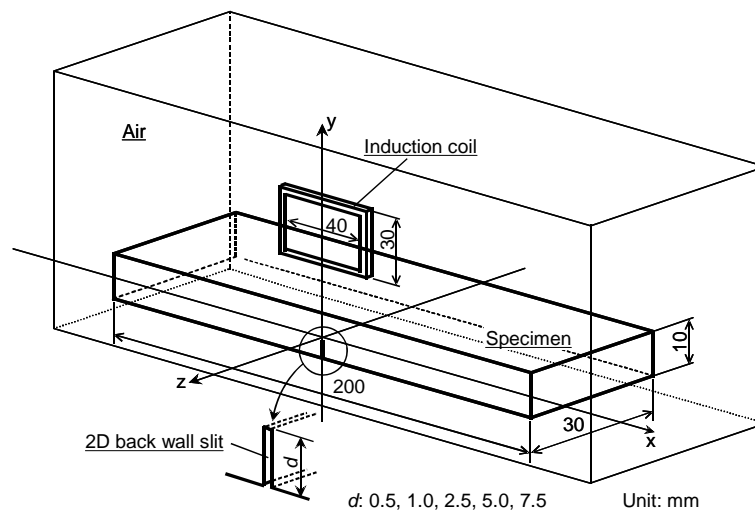


Fig. 3. Schematic illustrations of the FEA model with 2D back wall slit

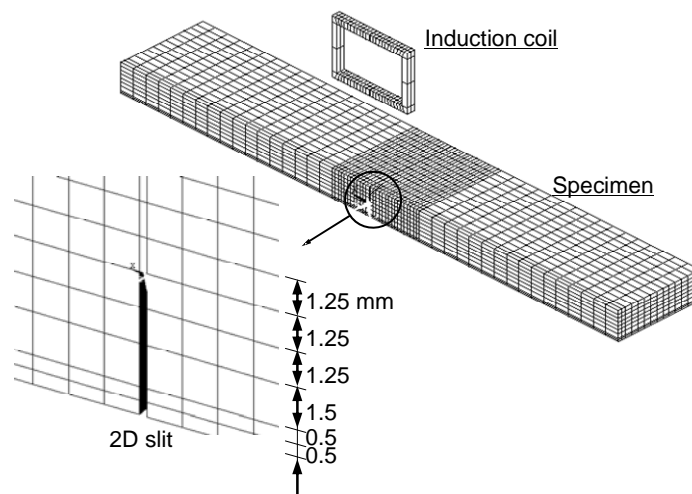


Fig. 4. Finite element mesh of the specimen containing 2D back wall slit and the induction coil

Table 1 Material properties

Type 304 SS (Specimen)	ρ	$70 \times 10^{-8} \Omega\text{m}$	
		μ_r	1.02
Copper (Induction coil)		μ_r	1.0
Air		μ_r	1.0

ρ : Electrical resistivity, μ_r : Relative permeability

3.2. Simulation results and discussion

Fig. 5 shows normalized PD (V/V_a) distribution calculated by FEA using the model containing 2D back wall slit with a depth of 5 mm. Distance between the PD pick-up pins is 5 mm and PD calculation interval is 2.5 mm. Alternating current frequency is 3 kHz which gives the maximum V_m/V_a for back wall slits in type 304 SS, where V_m is the maximum PD for the back wall slit and V_a is the PD calculated using the model without defects. As mentioned in section 2.2, PD distribution for back wall defect has a convex shape and the maximum PD is measured when the sensor is located just above the slit. As shown in Fig. 5, normalized PD distribution for the back wall slit shows a convex shape and the maximum V_m/V_a is calculated at the slit position.

Potential drop distribution around a surface slit with a depth of 5 mm was also calculated using the finite element mesh shown in Fig. 4. Similar PD distribution to that shown in Fig. 2(a) is calculated by FEA.

Accordingly, we can calculate PD distribution of the RICPD technique by FEA.

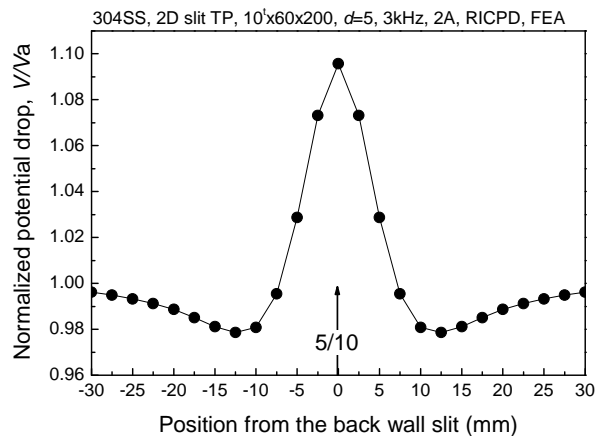


Fig. 5. Potential drop distribution around the back wall slit calculated by FEA

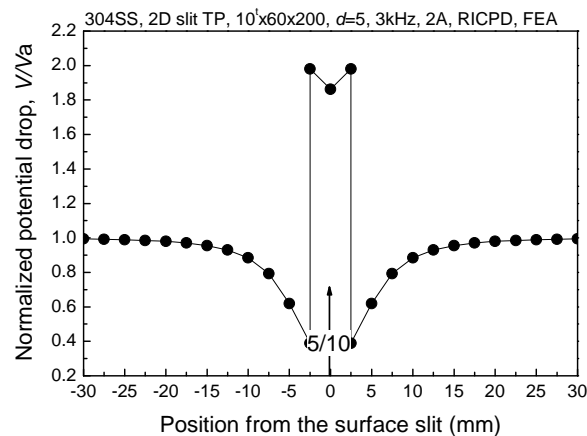


Fig. 6. Potential drop distribution around the surface slit calculated by FEA

In order to evaluate the applicability of the FEA to estimate the detection limit of the RICPD technique for the back wall defect size, calculated results were compared to those obtained by experiments. Fig.5 shows relationship between maximum normalized PD for each slit (V_m/V_a) and back wall slit depth (d). In the figure, both experimental and calculated results are indicated, and these results show good agreement, although the FEA results are slightly greater than those of experiment. Furthermore, no significant V_m/V_a is calculated for the slit with a depth of 0.5 mm, which is difficult to be detected by experiments. Correspondingly, we can estimate the detection limit of the RICPD technique in depth of back wall slits by FEA.

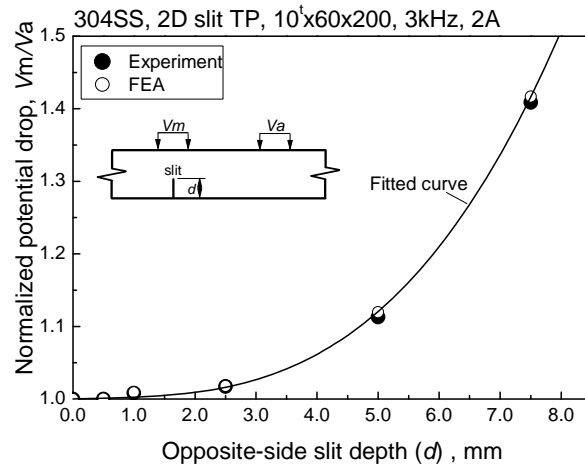


Fig. 7. Relationship between (V_m/V_a) and the depth of back wall slit

4. Experimental results and discussion

4.1. Detection and sizing of 2D surface and back wall slits in the paramagnetic material using the ICFPD technique

4.1.1. Surface slits

The size of the measured specimen of type 304 SS is 350 x 100 x 25 mm. The artificial defects are EDM (Electrical Discharge Machining) slits with a width of 0.3 mm, and depths of 1, 2.5, 5, 10, 15, and 20 mm. The distance between the two PD pick-up pins of the sensor used is 10 mm.

Fig. 8 shows the distribution of the PDs for each slit versus the distance from the defect position. The measuring interval was 1.0 or 5.0mm. The PDs are normalized by the average value of the PDs at no flaw region of the specimen (V_a). Each PD varies due to the existence of the defect. As explained in section 2.2, the PD gradually decreases as the sensor moves toward the slit until one of the PD pick-up pins of the sensor located just beside the slit, and then the PD jumps up when one of the PD pick-up pins crosses the slit. The PD distribution measured while the PD pick-up pins are across the slit shows U-shape. As shown in Fig. 8, the PDs measured on both sides of defect show almost the same value. That means the measurement repeatability is high enough to detect a small crack with a depth of 1mm. The lowest PD measured when one of the PD pick-up pins of the sensor located just beside the slit and the highest PD measured when one of the PD pick-up pins just crosses the slit are influenced by the depth of defect. Therefore, we use a ratio of the highest PD to the lowest PD, $V_{+\Delta/2}/V_{-\Delta/2}$, to evaluate the depth of the defect, where $V_{+\Delta/2}$ is the highest PD and $V_{-\Delta/2}$ is the lowest PD.

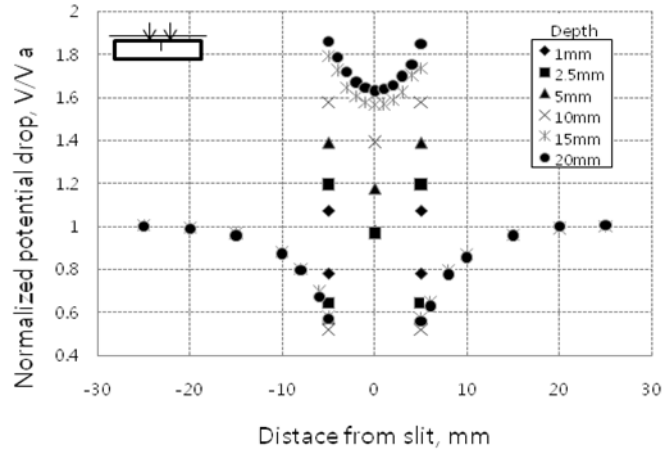


Fig. 8. Distribution of PDs for each surface slit in parent metal

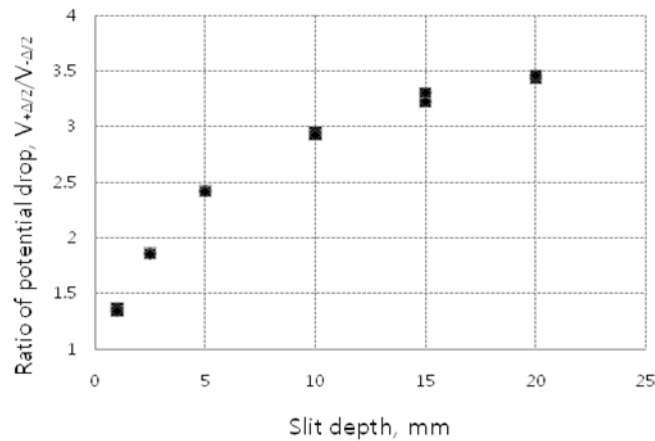


Fig. 9. Relationship between $(V_{+\Delta/2}/V_{-\Delta/2})$ and the depth of surface defects

Fig. 9 shows the parameter $(V_{+\Delta/2}/V_{-\Delta/2})$ versus the depth of surface defects. From the figure, $(V_{+\Delta/2}/V_{-\Delta/2})$ gradually increased as the depth increased. This tendency is similar to the results from the paramagnetic and ferromagnetic materials [9]. Therefore, we can use the parameter to estimate the depth of a surface defect, although the parameter is not linear with respect to depth.

4.1.2. Back wall slits

The artificial defects in the 25mm-thick specimen were EDM slits with a width of 0.3 mm and depths of 15, 20, 22.5, and 24 mm. The PDs were measured on the back wall with a same probe that was used to measure surface defects.

Fig. 10 shows the distribution of PDs, which are normalized using the average value of the PDs at no flaw region of the specimen (V_a), versus the distance from the defect position. The measuring interval was 1.0 or 5.0mm. As shown in the figure, the PDs in the vicinity of the defect gradually increases as the probe moves closer to the defect, and the PD on the position of defect shows a peak value. The peak values at the position of each defect are distinct with depths of the defects. This result means that the density of the induced current is strongly dependent on the thickness of the ligament that is the distance from the tip of the slit to the surface. The distribution of the PDs is symmetrical about the peak value at the position of the defect, and is clearly different from that of the surface slit (Fig. 8). Therefore, we are able to distinguish the type of defects by comparing the distributions of the PDs. The skin depth of SS is about 7.6 mm at a frequency of 0.3 kHz (relative permeability=1.02, conductivity= 1.43×10^7 S/m) [12]. In this measurement, defect with a depth of 15 mm, that is 10 mm in thickness of the ligament and is thicker than the skin depth, is possible to detect. The reason is that

the density of current disturbed by defect, while an induced current flows in the direction of thickness. The variation of the density influences the distribution of current on the surface on which the measurements were performed.

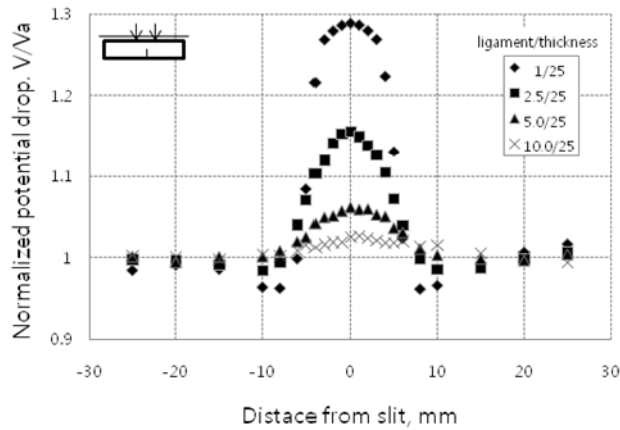


Fig. 10. Distribution of PDs for each back wall slit in a parent metal

Based on the PD distributions shown in Fig.8, we selected the parameter (V_m/V_a) to evaluate the thickness of the ligament. V_m represents the peak PD at the position of defect, and V_a is an average value of PDs in the sound area. Fig. 9 shows the parameter (V_m/V_a) versus the thickness of the ligament. The parameter (V_m/V_a) is obviously different with respect to the thickness of the ligament and decreases exponentially as the thickness of the ligament increases. Therefore, we can also detect an back wall defect, and estimate the thickness of the ligament from the PD distribution measured on the surface.

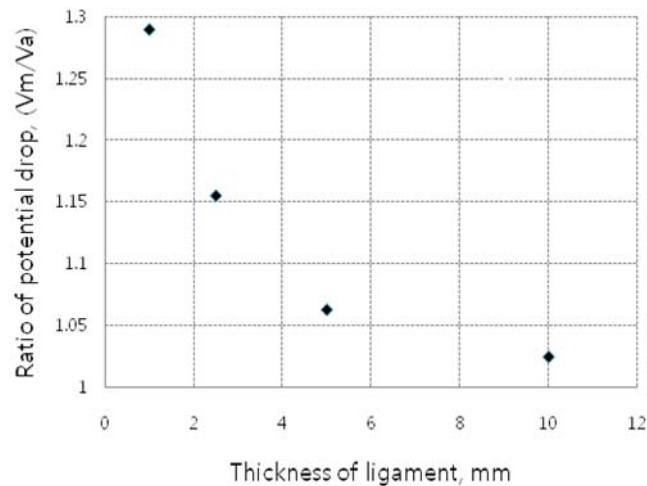


Fig. 11. Relationship between (V_m/V_a) and the thickness of the ligament

4.2. Detection and sizing of 3D surface slits in a weld joint of paramagnetic material using the ICFPD technique

The specimen (type 304 SS) described in this section is 200 x 140 x 10 mm in size and is welded with only one pass at the center of the specimen by laser welding. The weld metal zone is about 1.5mm high from the surface of the parent metal, and 4 mm in width. The 3D surface slits were made on the weld joint using EDM. The sizes of the surface slits are 0.5 mm in width, 10 mm in length and 1, 2, 3, 5, and 10 mm in depth. The slit with 10 mm depth is a through defect. As mentioned in section

2.1, typical ICFPD sensor consists of an induction wire which attached to the bottom of the rigid sensor case and a pair of pick-up pins. However, it is difficult to locate the typical ICFPD sensor on the surface of the specimen because of the bulge shape of the weld metal. Therefore, we attached a flexible thin copper plate with a width of 1 mm and a length of 70 mm on the surface of the welded specimen perpendicularly to the weld line as an induction wire. Potential drop measurements were performed using a commercially available sensor containing the PD pick-up pins with a distance of 10 mm.

Fig.10 shows the distribution of the PDs, which were normalized with respect to the average value of the PDs on the parent metal on the sound line for each slit (V_a), versus the distance from the defect position. The measuring interval was 1.0 or 5.0mm. In this figure, we show the PDs on the sound line in order to observe the variation of the PDs for the parent metal, the welded metal and the heat-affected zone (HAZ). In the sound line, the PDs in the 7 to 9 mm and -7 to -9 mm distance range, which is presumed to be in the HAZ, are smaller than those of the parent metal. The PDs in the welded metal (from -6 to +6 mm distance range) are greater than those of the parent metal. These appearances resulted from variations in the microstructure, and the bulge shape in the HAZ and weld joint. The distribution of the PDs on the sound line is symmetrical about the position of the defect, although the weld joint of the measurement line bulged. In the defect line, the PDs on the edge of the defect decrease, and the PDs in the defect zone have a U shape. These distributions are similar to the results of the surface defects in parent metal (Fig. 8). The PDs in the defect zone are higher than those on the sound line and differ with respect to the depth of the slits.

From the distribution of the PDs, the parent metal and the weld metal have different PDs because each metal has a different microstructure. Therefore, in order to estimate the defect in the welded zone, the effects of shapes and microstructure on the measured PD should be eliminated from the PDs. The parameter used to estimate the depth of defect in a weld is the ratio of PDs, $((V_{+\Delta/2} - V_{ws})/V_a)$, where $V_{+\Delta/2}$ is a peak PD at the defect zone, V_{ws} is the PD of the welded zone in the sound line, and V_a is the averaged PD of the parent metal in the sound line. Subtracting the PD of welded zone (V_{ws}) from the peak PD ($V_{+\Delta/2}$), the effects of shapes and microstructure of welded zone on the peak PD may be eliminated.

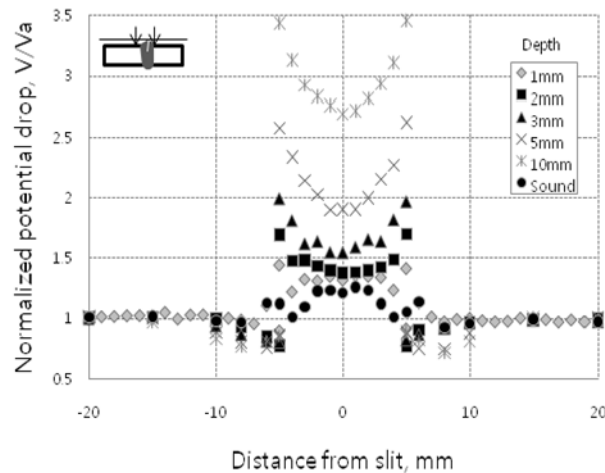


Fig. 12. Distribution of PDs for each surface slit within a weld zone

Figure 13 shows the ratio of PDs, $((V_{+\Delta/2} - V_{ws})/V_a)$, versus the depth of the defects. The values increase as the depth of the defects increase. Therefore, we can use the ratio of the PD to estimate the depth of the surface defect in a weld.

According to the results described in 4.1 and 4.2, the ICFPD technique is able to estimate both the defects in the homogeneous metal and defects in the areas with varied microstructure such as a weld joint.

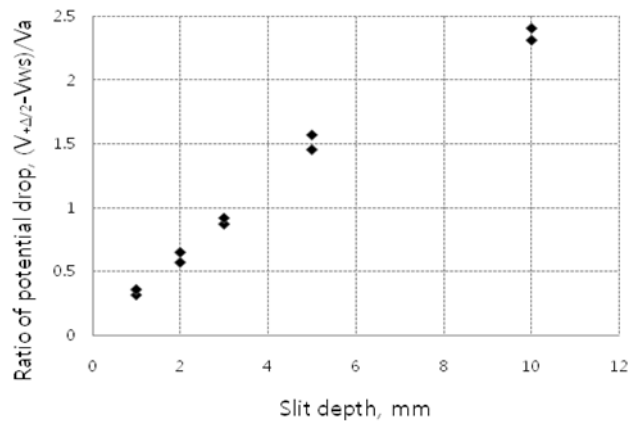


Fig. 13. $((V_{+\Delta/2} - V_{ws})/V_a)$ versus the depth of the surface slit in a weld joint

4.3. Detection of cracks in components using the PD technique based on electromagnetic induction

The preceding experiments estimate artificial defects created in parent and weld metals using EDM. However, field components have various bulk and shapes, and defects vary in size and shape, unlike artificial defects. Thus, we inspected defects in welds in field components containing cracks to verify the applicability of the PD techniques based on electromagnetic induction.

4.3.1. Detection of cracks in a weld between a valve and a pipe using the ICFPD technique

The specimen inspected consists of a weld between a valve and a pipe. The valve and pipe are made of type 321 and 304 SS, respectively. An inspection line is on the HAZ, 6 mm away from the weld. The PDs were measured with a scanning interval of 1 or 5 mm as a probe moved in a circumferential direction. The measurement conditions were a frequency of 0.3 and 10 kHz, 2A current, and 90 and 70 dB gain. The probe utilized was the same as that used for weld defects.

Fig. 14 shows PDs versus probe position in circumferential angle. Both distributions of PDs measured at the frequencies of 0.3 kHz and 10 kHz are similar in shape, and defect indications are observed at positions of 75, 83, 98, and 155°. According to the shape of the distribution, the defect at 75° is identified as a surface crack, and the defect at 155° is identified as an back wall or internal crack.

After the measurement, the specimen was cut along the inspected line and the cross section was examined. Fig. 15 shows the cross section of the specimen. From the photo, we find that the defect at 75° is a surface crack, and defects at about 83, 95, and 150° are internal cracks. Comparing the defect indications in the distribution of the PDs with the actual defects observed on the cross section, positions and variety of detected defects are in good agreement, but the positions for each defect have a small difference.

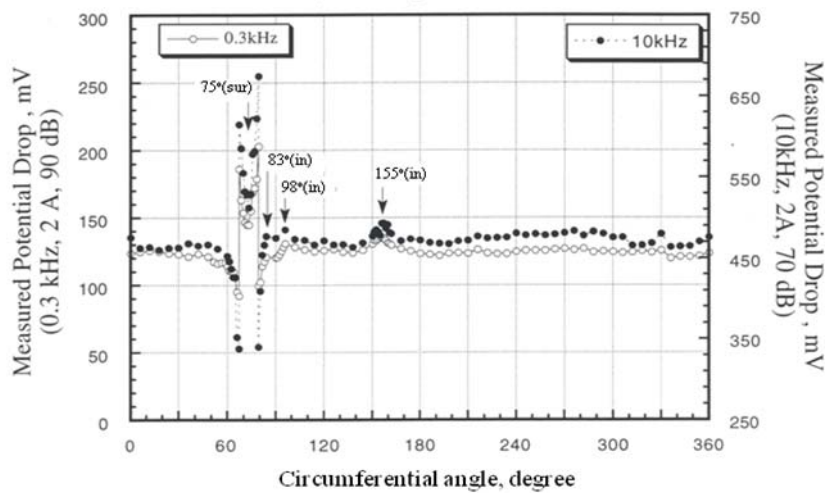


Fig. 14. Distribution of PDs versus circumferential angle for the specimen

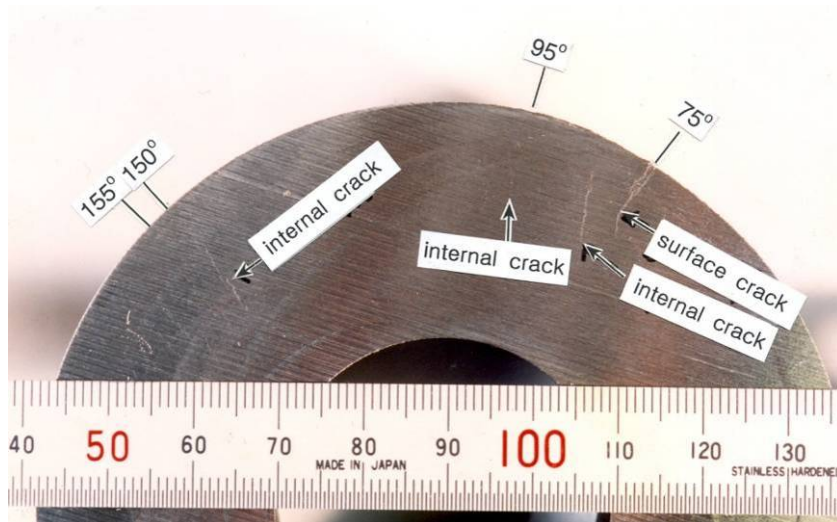


Fig. 15. Photo of the cross section of the specimen

4.3.2. Detection of simulated stress corrosion cracks in dissimilar metal weld using the RICPD technique

As mentioned above, the PD technique based on electromagnetic induction is useful to detection and sizing of defects in conductive materials. The technique was applied to the international round robin test program called as Program for the Inspection of Nickel-alloy Components (PINC program). The PINC program was organized by the U.S. Nuclear Regulatory Commission (NRC) and aimed to determine the effectiveness of a variety of nondestructive testing techniques for the detection of stress corrosion cracking through a series of round robin tests (RRT). Details of the PINC program are described in the literatures [13, 14]. In this section, results of blind tests, which were conducted as one of the RRT of the PINC program, obtained on dissimilar metal weld specimens using the RICPD technique are presented. In the blind tests, only the information that the simulated stress corrosion cracks are on the internal surface of the weld metal is given to the inspectors prior to the measurements.

Photos of the specimens used for the blind test are shown in Fig. 16 with the specimen numbers of

PINC2.9 and PINC2.10 defined by the program. As illustrated in Fig. 17, the specimens consist of nozzle to safe end dissimilar metal welds.

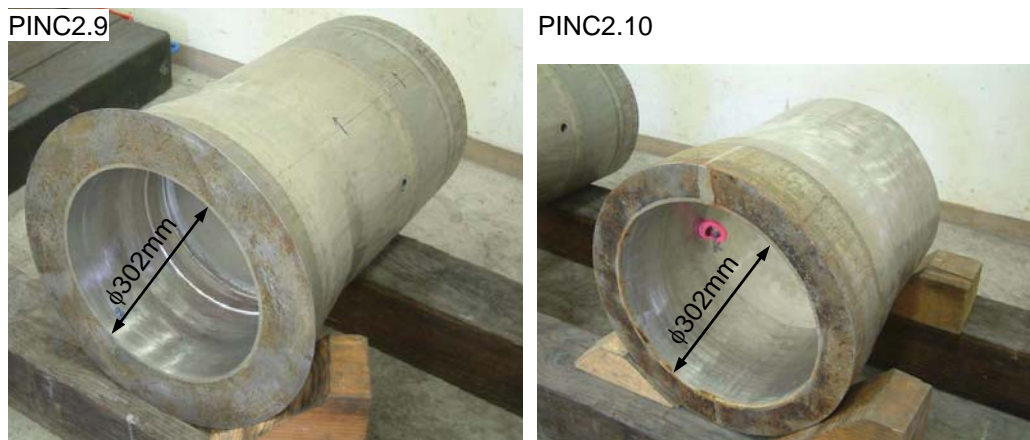


Fig. 16. Photo of the specimens used in the RRT of the PINC program [14]

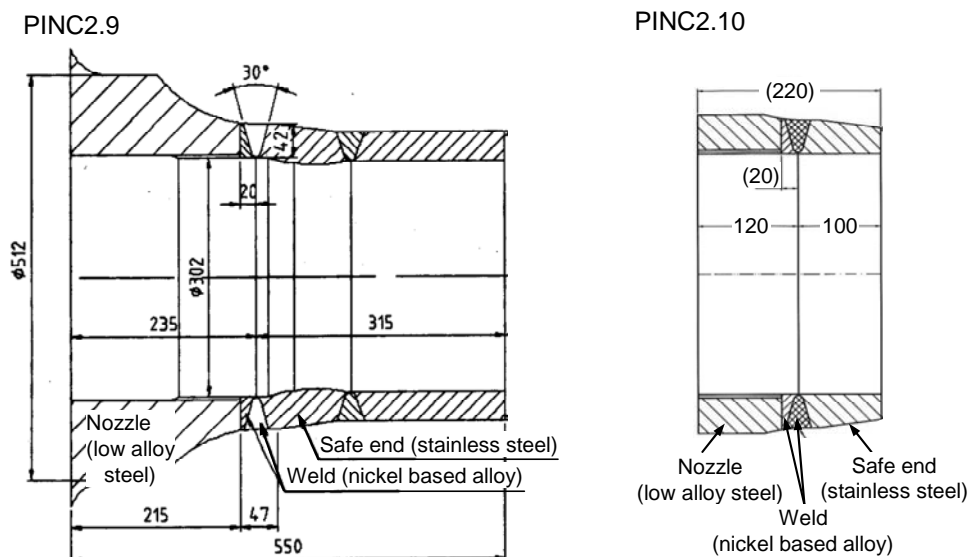


Fig. 17. Schematic illustrations of cross section of the specimens [14]

The RICPD sensor used in the test was same as that shown in Fig. 1(b). Distance between the two PD pick-up pins is 5 mm. Alternating current supplied to the induction coil was set to 3 kHz and 2 A, which was optimized to detect surface breaking defects by FEA performed prior to the measurement.

Since the cracks were introduced on the internal surface of the weld metal of the specimen, the measurements were performed on this surface. Measuring lines were drawn on the surface prior to the measurements. The lines were parallel to the weld line inspected and set at 2.5 mm interval. A flexible ruler for a sensor guide was put on the surface aligned with the measuring line. Position of the sensor was defined by identifying the flexible ruler.

At the beginning of the measurements, crack orientation was assumed to be axial or circumferential directions of the specimen. According to this assumption, sensor arrangement was defined as follows; for detection of axial cracks, which are perpendicular to the weld line, the sensor is scanned along the measuring line with the longest edge of induction coil aligned with the scanning direction, and for detection of circumferential cracks, which are parallel to the weld line, the sensor is scanned along the pre-defined measuring line with the longest edge of induction coil perpendicular to

the scanning direction (Fig. 18). In this inspection, a target defect length was decided to be more than 5 mm because of the limitation of measurement time. Based on this target defect length, detection interval was defined as 5 mm.

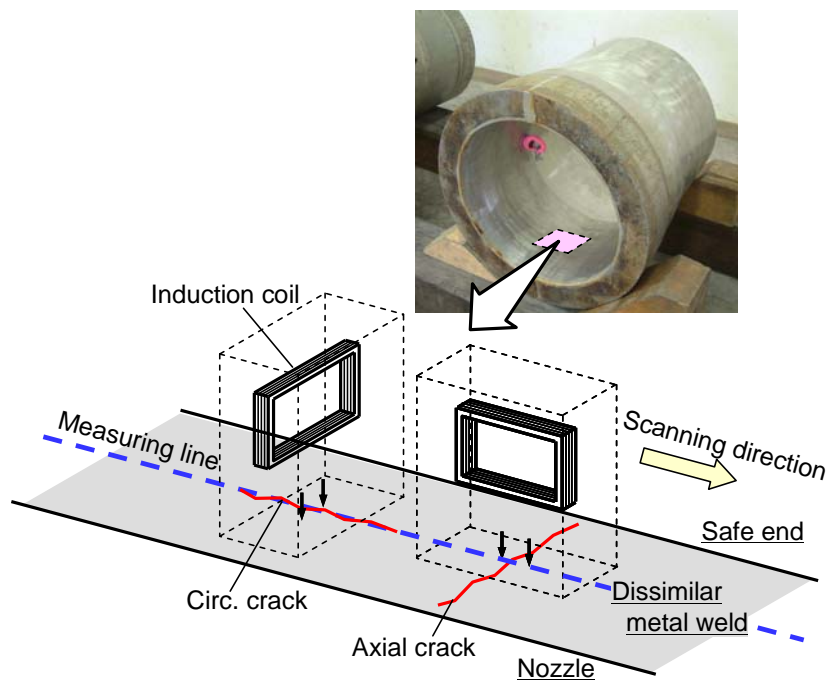


Fig. 18. Schematic illustration of sensor arrangements for detection of circumferential and axial cracks

The blind test results are presented in the final report of the PINC program [14]. According to the report, measured potential drop data were analyzed by a data analysis group to determine the effectiveness of the RICPD technique. Inspection plots of the RICPD technique for each of the two specimens are shown in Fig. 19. The figure is originally presented in the final report and is slightly modified to make it clearer to understand. The horizontal axis is the outer circumferential position of the specimen and the vertical axis is the axial position started from the center of the weld line. Hatched rectangles indicate true defect locations with a 10mm tolerance, blank rectangles show the estimated defect locations according to the PD distribution measured using the RICPD technique, and cross hatched rectangles indicate undetected defect locations. From Fig. 19, 8 cracks are detected and 4 cracks are undetected in PINC2.9 specimen in which total 12 cracks are introduced. On the other hand, all of the cracks in PINC2.10 specimen are successfully detected although the indicated locations are slightly different from the true defect locations. Detected crack orientations were estimated using the PD distributions to be circumferential direction in the PINC2.9 specimen and axial direction in the PINC 2.10 specimen. Comparing the estimated crack orientations with the released information about cracks after the RRT, the estimations were correct for all of the detected cracks. In addition, it was revealed that the orientations of the undetected cracks in PINC2.9 specimens were circumferential directions.

For the detection of circumferential cracks, the induced current distribution is affected by the material properties of nozzle, weld metal, and safe end because the induced current flows in axial direction, unlike for the detection of axial cracks. Accordingly, the measured potential drops for detection of the circumferential cracks include the effect of these materials, and consequently, detectability for circumferential cracks decreased. Moreover, in the RRT, coarse measurements were conducted using relatively large sensor compared to the size of the weld to cover all of the surface of the weld line, and therefore, few PDs generated from the cracks were measured.

Fine measurements to gain many PDs from cracks using an automated measuring system with multiple pin sensors and/or small sensors can improve the detectability of circumferential cracks.

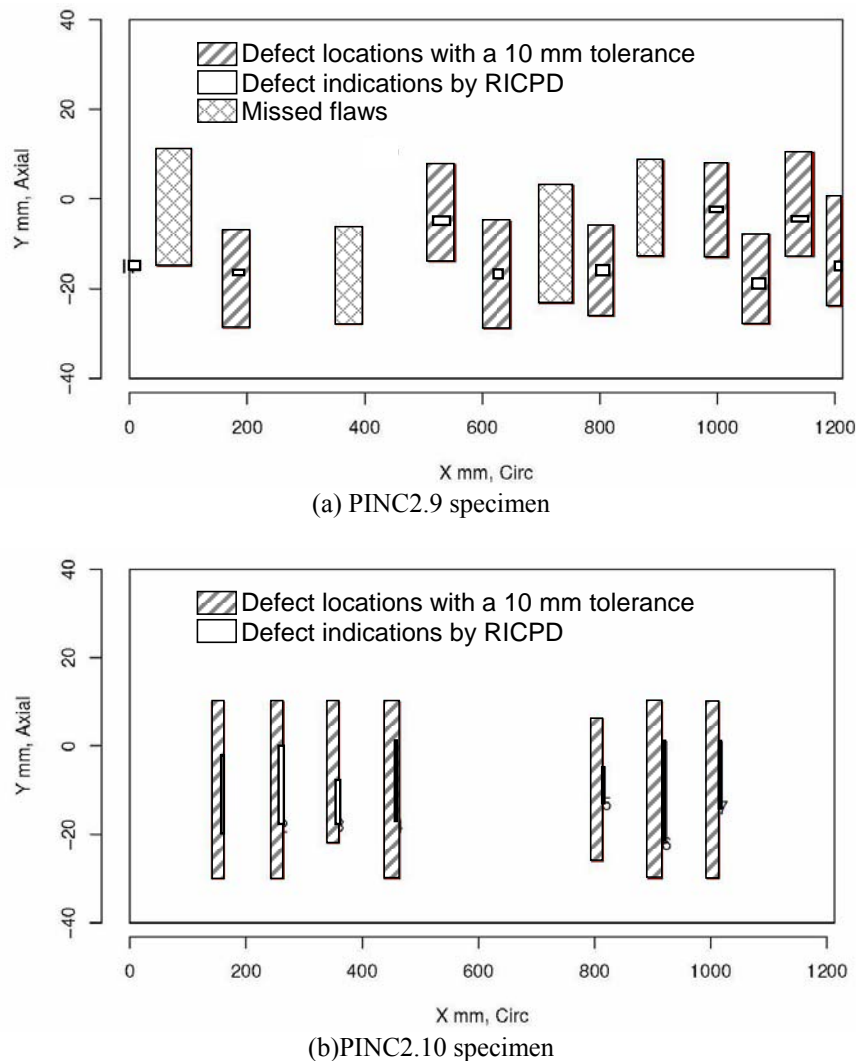


Fig. 19. Detection capability of the RICPD technique [14]

5. Conclusions

To investigate the applicability and usefulness of the PD techniques based on electromagnetic induction, FEA results of the RICPD technique are firstly presented, followed by some experimental results for detection and sizing of defects using the techniques of ICFPD and RICPD. The following conclusions can be drawn from the results:

- 1) Experimental and FEA results for the RICPD technique show good agreement and detection limit of the technique in depth of back wall slits can be estimated by FEA.
- 2) The PDs measured using ICFPD technique around surface defects in parent and weld metals are varied with the depth of defects, and the ratios of PDs measured nearby the defect increased as the depth of defects increased. The ratios of the PDs can be used for quantitative estimation of the depths of surface defects.
- 3) The ICFPD technique can be used to investigate defects in both parent and weld metals. By comparing the distributions of the PDs, surface defects and back wall defects can be distinguished by the ICFPD technique.
- 4) Most of the cracks in the components investigated are successfully detected by the ICFPD and

RICPD techniques.

- 5) Fine measurements to gain many PDs from cracks using an automated measuring system with multiple pin sensors and/or small sensors can improve the detectability of defects.

References

- [1] T. Shoji, Current statures and future direction of potential drop method for QNDE, *Journal of the Japanese Society for Non-destructive Inspection (in Japanese)*, Vol. 49, No. 11, (2000), pp. 759-766.
- [2] ASME Boiler and Pressure Vessel Code Section III, Division 1, 1977 Edition, American Society of Mechanical Engineers, (1977).
- [3] H. Kim and E. Na, A study on the non-contact detection technique of defects using AC current - The influence of frequency and lift-off-, *Journal of the Korean Society for Nondestructive Testing* Vol.22, No.1, (2002), pp. 53-58.
- [4] H. Kim and T. Shoji, The detection of defects in paramagnetic materials using locally focused electromagnetic field technique, *key Engineering Materials*, Vols. 270-273, (2004), pp. 625-629.
- [5] H. Kim, The evaluation of surface crack in paramagnetic material by FEF technique, *Journal of the Korean Society for Nondestructive Testing*, Vol.24, No.5, (2004), pp. 532-537.
- [6] M. Saka, D. Yuasa, H. Abe, K. Sugino and H. Kageyama, Potential Drop technique for nondestructive evaluation of bifurcated crack in rail, *Nondestructive Testing and Evaluation*, Vol. 10, No. 6, (1993), pp. 333-341.
- [7] W.D. Dover, F.D.W. Chalesworth, K.A. Taylor, R. Collins and D.A. Michael, AC field measurement –theory and practice, *The measurement of crack length and shape during fracture and fatigue*, C.J. Beevers, EMAC, Wiley, West Midlands, UK(1980), pp. 222-260.
- [8] H. Kim and T. Shoji, Study on induced current focusing potential drop (ICFPD) technique – examination of the sizing accuracy of defects and its frequency dependence- (in Japanese), *Journal of the Society Materials Science Japan* Vol. 43, No. 494, (1994), pp. 1482-1488.
- [9] H. Kim, T. Shoji and S.H. Chung, Nondestructive evaluation of 2-dimensional surface crack in ferromagnetic metal and paramagnetic metal by ICFPD technique, *Journal of the Korean Society Mechanical Engineers* Vol. 19, No. 5, (1995), pp. 1202-1210.
- [10] Y. Sato, T. Atsumi, T. Shoji, Continuous monitoring of back wall stress corrosion cracking growth in sensitized type 304 stainless steel weldment by means of potential drop techniques, *International Journal of Pressure Vessel and Pipings*, Vol. 84, (2007), pp. 274-283.
- [11] Y. Sato, T. Atsumi, T. Shoji, Application of induced current potential drop technique for measurements of cracks on internal wall of tube-shaped specimens, *NDT & E international*, Vol. 40, (2007), pp. 497-504.
- [12] W.H. Hayt, *Engineering Electromagnetic*, 5th edition (1990), McGraw-Hill, Chapter 8.
- [13] K. Kono, T. Takagi, N. Chigusa, Overview of the Program for the Inspection of Nickel-alloy Components (PINC) (in Japanese), *Maintenology*, Vol.6, No.1, (2007), pp. 67-69.
- [14] S.E. Cumblidge, S.R. Doctor, P.G. Heasler, T.T. Taylor, I. Prokofief, Results of the Program for the Inspection of Nickel Alloy Components, NUREG/CR-7019, (2010).